*Journal of Applied Electrochemistry* **31**: 1389–1394, 2001.



# Chromic acid regeneration process with fuel cell electrode assistance. Part II: Electrochemical characterization, material compatibility and energy consumption

M.I. AHMED, T.M. HOLSEN[†] and J.R. SELMAN*
*Department of Chemical and Environmental Engineering, Illinois Institute of Technology, Chicago, IL 60616, USA*
[†]*Present address: Department of Civil and Environmental Engineering, Clarkson University, Potsdam, NY 13699, USA*
*(*author for correspondence)*

Received 22 December 2000; accepted in revised form 17 August 2001

**Abstract**

Electrochemical characteristics, energy consumption and material compatibility aspects of a novel process for regeneration of spent hard chromium plating baths using a Nafion-117 separator and a fuel cell cathode are discussed. Electrochemical impedance spectroscopy (EIS) and stationary polarization curves were used to characterize the performance of a fuel cell cathode in the regeneration cell. The configuration of the MEA, current collector, and flow distributing backing plate may, during long-term operation, lead to excessive ohmic resistance, which necessitates a special design of the cathode assembly. X-ray diffraction indicated that Cu, Fe, Ni, and Cr were deposited on the electrode matrix, leading to deactivation of the Pt-catalyst. The deactivation causes a rising cell voltage during electrolysis. Nevertheless, the energy consumption of the regeneration cell is at least 1 V less than that of a comparable cell with hydrogen evolving cathode.

## 1. Introduction

Increasingly stringent environmental regulations are a strong incentive to search for novel processes that regenerate hard chrome plating baths *in situ* by continuously removing metallic contaminants such as Cu, Fe, and Ni as well as Cr(III) ions. We recently described the concept of a regeneration cell incorporating a fuel cell cathode, and reported the results of a lab-scale cell using a simulated plating bath as electrolyte (M.I. Ahmed et al., submitted).

Cost effectiveness is an important aspect of developing a new process and, of course, lower energy consumption is a major advantage for a new process. Energy consumption must be balanced with the capital costs of the processes including the cost of construction materials since the acidic environment of a hard chromium plating solution requires highly stable and hence expensive materials. While electrodes and cells can be designed to minimize power losses caused by inhomogeneous current distribution, ohmic resistance, side reactions and capital cost depend ultimately on cell resistance and material stability. For example, in cells using fuel cell electrodes, disintegration of the electrode backing (functioning as a current collector) lowers the electronic conductivity, increases the cell resistance, and hence increases energy consumption. Thereby operating costs as well as capital cost are increased. Electrochemical characterization may help to understand the nature and cause of material incompatibility and lead to a properly designed, inexpensive cell as well as peripheral equipment.

In this work, we report results obtained while investigating a novel process for regeneration of spent hard chromium plating baths using a Nafion-117 separator and a fuel cell cathode. In Part I of this series (M.I. Ahmed et al., submitted), contaminant elimination rates were reported and the mechanisms of their removal analyzed. In this paper we report electrochemical characteristics, material compatibility and energy requirements of the process.

## 2. Experimental

The experimental cell and reaction schematic are shown in Figure 1. The porous cathode consists of a Pt-black/carbon catalyst layer (electrode matrix) on one face of a Nafion-117 membrane in contact with a current collector (backing), which, in turn, is in contact with a graphite block with a serpentine air channel milled into it. The clear side of the Nafion-117 contacts the electrolyte (spent plating bath) on the catholyte side of the lab-scale cell. In the anolyte compartment a lead plate is used as the anode.

The electrochemical and energy performance was evaluated by analyzing the measured anode, cathode, and cell voltage during experiments. An additional experiment was carried out under anoxic conditions. Stationary polarization curves and AC impedance

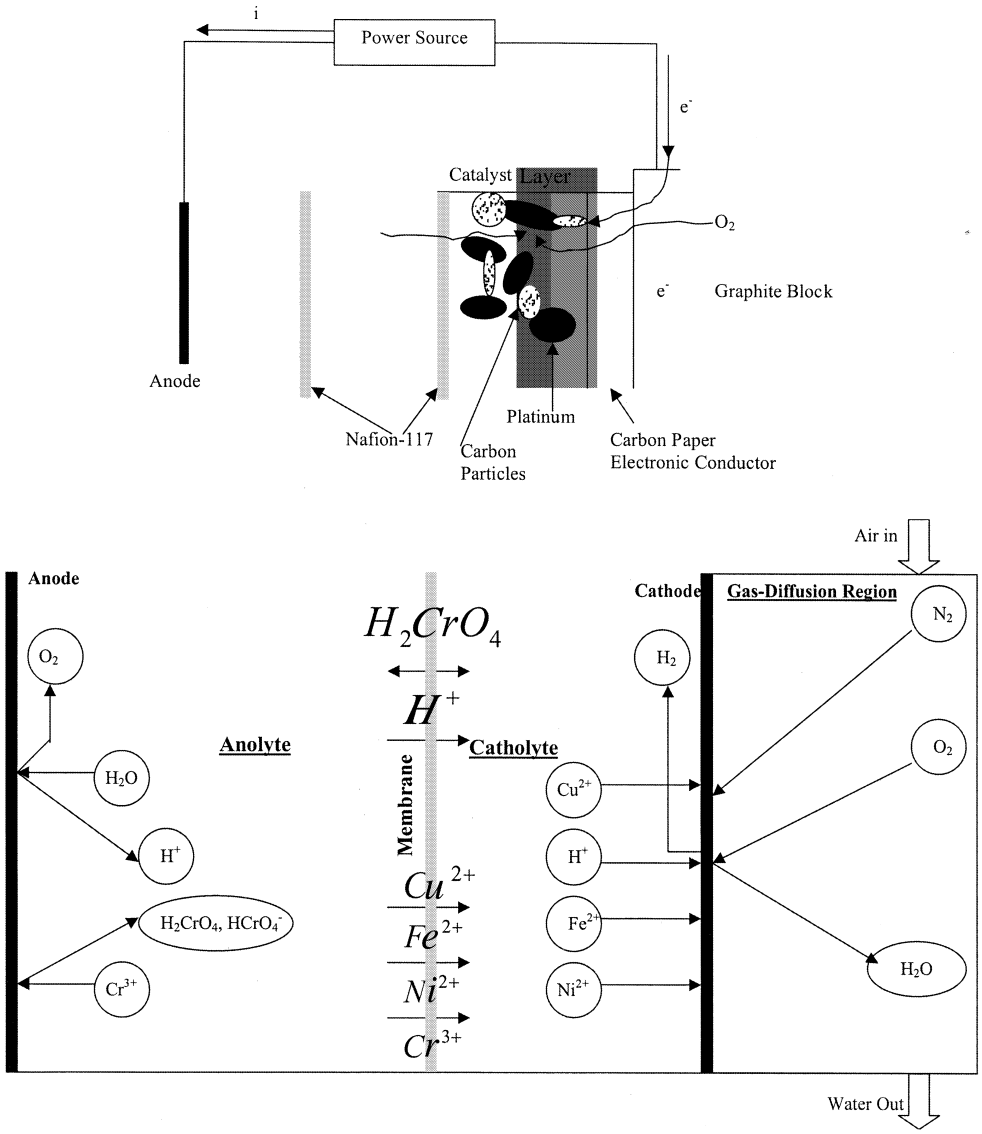


*Fig. 1.* Schematic representation of the reaction system in FCMP cell, and electron flow.

spectra were measured to evaluate the cathode performance and limitations. This is in addition to X-ray diffraction of the cathode catalyst.

The applied current was generated and the cell voltage measured by an EG&G Potentiostat/Galvanostat model 173A. The electrode voltages were measured with respect to a standard calomel electrode (SCE) that was left in solution only during measurement. In long-term exposures, a $Hg/HgSO_4$ reference electrode was used.

Steady-state polarization curves were measured using the same EG&G potentiostat. A.C. impedance characteristics where obtained using a Solarton S1287 electrochemical interface and S1255 HF frequency response analyzer interfaced to the computer through Corrware and Zview softwares.

X-ray diffractograms were obtained using a Rigaku Miniflex X-ray diffractometer with data-acquisition software. All experiments were carried out at room temperature.

## 3. Results and discussion

### 3.1. *Performance of the oxygen gas diffusion electrode with Pt-catalyst under stationary polarization*

The polarization curves shown in Figure 2 were obtained in sulfuric acid (3.0 N, pH $<$ 0), and contaminated 2.5 M chromic acid. In both solutions polarization curves were obtained while either supplying air/$O_2$ (120 $cm^3$ $min^{-1}$) or operating under anoxic conditions after purging with argon for about 6 h. The corresponding a.c. impedance diagrams (Cole–Cole plots) are shown in Figure 2.

In both cases there is a region at higher cathodic potentials beyond which the polarization curves become parallel. In that region, the *I–V* curves for operation under air compared to operation under argon are separated by 1.15 V in the case of sulfuric acid. The separation is larger in the case of chromic acid. This

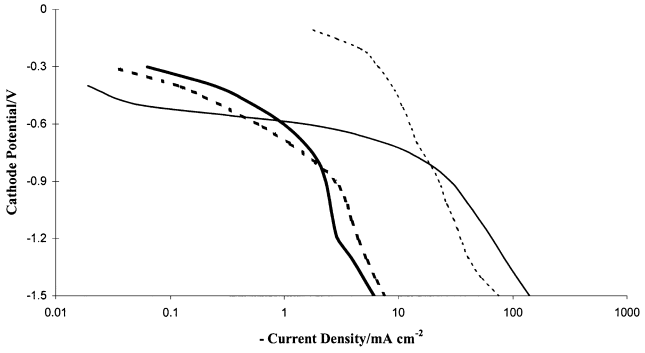


*Fig. 2.* Cathode polarization curves in contaminated chromic acid and sulfuric acid, while air or argon is supplied. The catalyst loading is 4.9 mg $cm^{-2}$ Pt-black on carbon. (—) chromic–Ar, (—) chromic–O, (– –) sulfuric–Ar, (- -) sulfuric–O.

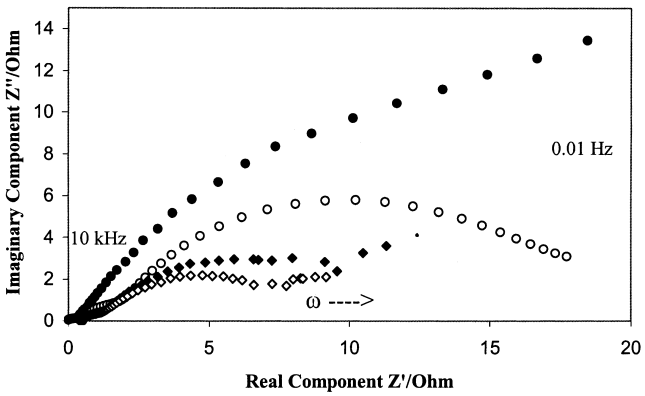


*Fig. 3.* A.c. impedance diagrams (Cole–Cole plots) of oxygen gas diffusion electrode (4.9 mg Pt-black $cm^{-2}$) in various solutions. (●) sulfuric–Ar, (○) sulfuric–O, (◆) chromic–Ar, (◇) chromic–O.

indicates energy savings of approximately 0.01 J $cm^{-2}$ $s^{-1}$ cathode at 10 mA $cm^{-2}$.

The permeation of electrolyte through the membrane into the porous electrode matrix results, upon electrolysis, in a mixed potential at the cathode, with a significant loss in oxygen reduction performance and also poor fuel utilization. This is obvious from the cell open circuit potential (Figure 2). While the open circuit potential is 1.2 V in sulfuric acid (1.0 N), the maximum obtained in contaminated chromic acid was 1.0 V. The polarization curves appear to indicate mixed ohmic-kinetic control with a double valued Tafel slope. At much higher current density, perhaps at 800–1000 mA $cm^{-2}$ in air at 1 atm, one would expect mass transfer limiting behavior only [1, 2]. If such a limiting behavior did not occur it would be possible to save more energy by operating at such high current densities, and thereby improve the system engineering requirements.

### 3.2. *Cathode a.c. impedance (EIS) characterization*

Electron and ion flow during application of current is illustrated schematically in Figure 1. The electrolyte/electrode interface is characterized by the double layer capacity of the solution in the pores. Its impedance changes due to change in the double layer composition as well as concentration gradients.

EIS experiments (Figure 3) confirmed the conclusions of Springer et al. [3] that the main characteristics of the cathode a.c. impedance are a high frequency loop, representing the kinetics at the cathode/electrolyte interface and a low frequency loop representing diffusion limitation. Springer et al. [3], Giureanu and Wang [4] ascribed the latter to diffusion resistance of gaseous reactants through the backing.

In general, decrease of oxygen partial pressure in the cathode of a fuel cell will reduce its performance due to reduction in the cathode potential. Also, electrolyte permeation, together with water production at the cathode, may lead to increased transport resistance of oxygen and decreased oxygen partial pressure at the reaction site. This would explain the appearance of the low frequency loop and agrees with the emergence of a mass transfer resistance at high current density, as shown in the polarization curves of Figure 2.

Obviously, from the size of the high frequency loop (Figure 3), the kinetics are faster for hydrogen evolution than for oxygen reduction. This works in tandem with the high permeability of the Nafion-117 membrane to protons, in addition to the very low pH. However, the kinetics for oxygen reduction are faster when sulfuric acid is used rather than chromic acid (Figure 3). This finding is in agreement with the mixed potential explanation given previously (Section 1). An important feature is the appearance of the low frequency loop in the case of argon-purged solutions. This agrees with the fast kinetics of the $H_2$ evolving cathode, which works in tandem with proton diffusion through the Nafion-117 membrane.

### 3.3. *Electrode deactivation*

#### 3.3.1. *Effect of long-term use*

A considerable degree of kinetic deactivation was encountered which is of concern because of the costly catalyst used. Figure 4 shows the polarization of the fuel cell oxygen cathode in the range −5 to 5 V in sulfuric as well as contaminated chromic acids. These polarization curves compare the performance of the cathode before

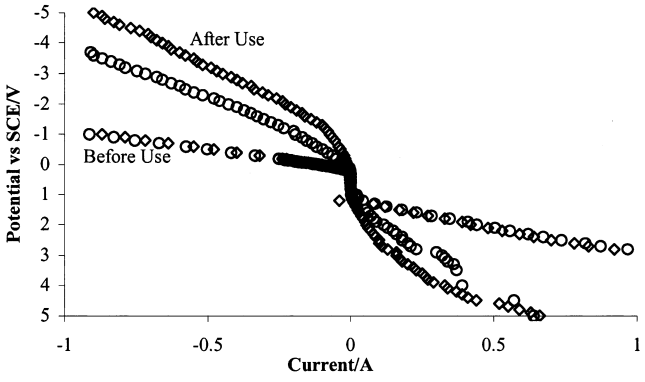


*Fig. 4.* Polarization curves of the fuel cell cathode (4.1 mg $cm^{-2}$ Pt-black on carbon), before and after use for 3 days. (◇) sulfuric acid 3.0 N, (○) contaminated chromic acid.

and after use in the removal experiments. Mass transfer limiting behavior is evident after long-term use.

Kinetic limitations may lower the cathode potential appreciably. Therefore, although the potential at which the fuel cell cathode works in the cell is theoretically too positive to allow metal deposition, the actual potential is in the range where metals could be deposited [5]. Metal impurities deposited on the MEA catalyst would decrease the catalytic ability of the MEA for oxygen reduction and thereby accelerate the naturally occurring process of deactivation by sintering or dissolution/deposition of the smallest Pt-particles as discussed below. However, it may not affect the contaminant removal rates (see Part I, [M.I. Ahmed et al., submitted]).

### 3.3.2. *Mechanisms of deactivation*

Possible contamination due to corrosion of the lead anode is limited since solid lead sulfates or chromates are likely to form at the pH of the bath and under operating currents. Production of protons due to reoxidation of trivalent chrome keeps the solution pH below zero. This is good for prevention of deposition or precipitation; on the other hand it decreases the current efficiency.

In the present work we investigated the deactivation mechanisms by comparing the X-ray diffraction patterns of the electrode before and after use. Figure 5 shows the diffraction patterns of Pt-black supported on Vulcan carbon. Of course, some platinum oxide is present due to air exposure; however, no contribution to X-ray diffraction is evident since the oxide is reportedly amorphous [6]. A uniform shift of about 0.4° in all peaks was observed after use, which is considerable. In addition, sintering at 1000 °C reveals that some peaks are related to metal plating at the cathode. These peaks could not be seen at normal temperature since metal deposition at room temperature yields an amorphous product.

It may be useful to briefly review the literature on the causes of deactivation of fuel cell electrodes. Kunz [7] has stated that oxygen reduction kinetics depend on differences in the activity between smooth and high surface area platinum. These result from a crystallite size effect that has been found to be present in high surface area platinum (Pt-black).

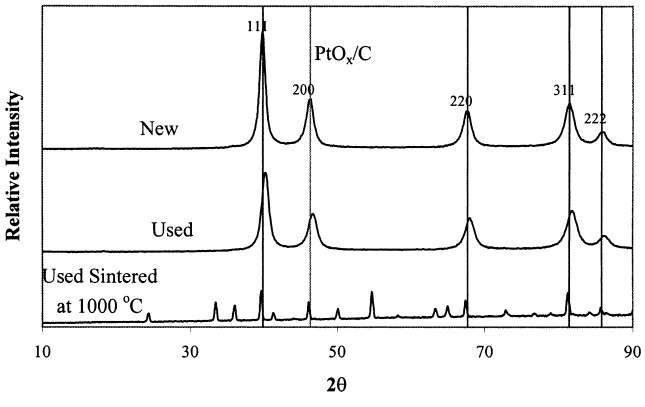


*Fig. 5.* X-ray diffraction of oxygen fuel cell electrode (4.1 mg cm$^{-2}$ Pt-black on carbon) before and after use in a removal experiment. (—) O.C.V, (–■–) operating at 0.2 Å.

In summary, deactivation may be attributed to:

1. Electrode flooding, leading to oxygen diffusion limitation.
2. Corrosion of the carbon support due to acidic flooded conditions, parasitic hydrogen evolution, and local heating effects.
3. Platinum catalyst loss by dissolution, e.g., in chromic acid.
4. Failure to maintain Pt-catalyst dispersion due to matrix (carbon) dissolution. In the case where all atoms in the crystallite are at the surface, 100% dispersion of the metal would have been achieved [8], but this could only be accomplished by very small particles, which causes matrix dissolution and could lead to flooding.
5. Loss of platinum surface area due to sintering. As discussed by Kinoshita [9], sintering involves a decrease in intraparticle distance and hence densification. It leads to loss of surface area and porosity. One cause of sintering could be the relatively high operating potential, since polarization causes localized heating.

Alloying of Pt with non-noble metals is relevant to our investigation and may be responsible for catalyst deactivation. The predominant $Pt_3M$ phases (M = Cr, Cu, Fe, Ni, Co) present in the alloys have f.c.c crystal structures [7, 10]. Alloying of Pt with each of the transition metals causes a contraction in the lattice parameters and an increase in particle size in the order Pt < Pt + Ni < Pt + Cr [11]. The decline of PAFC cathodic activity, in successive cycles with time, may be inferred from failure to maintain Pt-dispersion [8, 12]. Pt clusters aggregate during reaction, leading to a decrease of the metal surface and hence the catalytic activity. According to Lin [12], after six cycles of electrochemical testing the Pt–Pt coordination number increased from 5.51 ± 0.18–6.05 ± 0.16 Å. The average particle size of a fresh catalyst was 32 Å (the same as for our MEA) and increased to 45 Å after cycling [12]. This could be due to the reduction of the partially oxidized Pt-atoms.

### 3.4. *Exploration of alternative cathode configurations*

An important potential cause of cell failure is the disintegration of the porous cathode backing material and, eventually, of the carbon graphite block, whose surface is adjacent to the backing. Both of these lead to a rise in the cell voltage (Figure 6) as the ohmic resistance increases due to inadequate contact between the electrode (MEA) and the current collector (graphite block). In preliminary experiments we found that disintegration of the graphite block takes place over time, although rather slowly in a well-designed electrode. We attribute the disintegration to the hydrogen evolution on the graphite surface contacting the MEA,

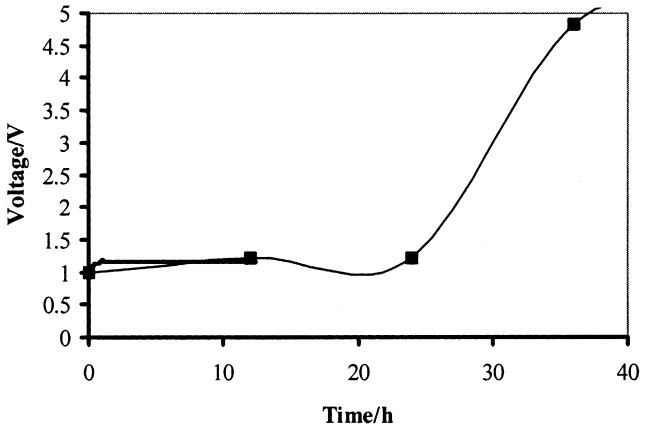


*Fig. 6.* Cathode voltage during operation at 0.2 Å with the original cathode configuration.

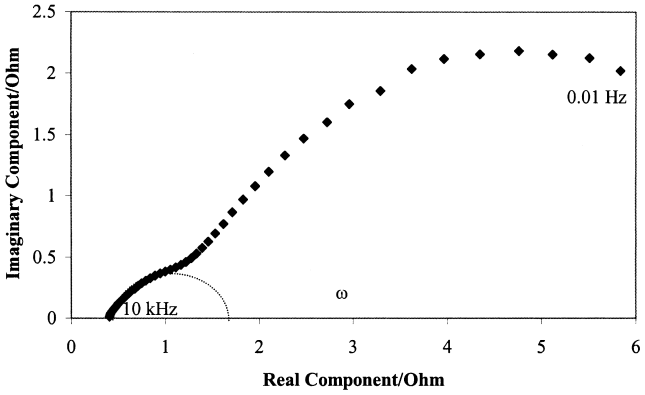


*Fig. 8.* A.c. impedance diagram (Cole–Cole plot) of the fuel cell cathode with the new configuration in contaminated chromic acid.

as the electrode becomes flooded due to mechanisms discussed in Section 3.3 above.

As mentioned in Part I of this paper (M.I. Ahmed et al., submitted), reconfiguring the electrode may resolve this problem. For example, a cut may be made through the backing material and this cut filled with folded platinum gauze, while the rest of the backing remains as originally designed. This reconfiguration serves three purposes; (1) it improves the platinum–carbon contact leading to less ohmic resistance within the electrode; (2) it facilitates water convection through the electrode to the gas stream due to the much larger gauze porosity and (3) it increases platinum loading (originally 5.0 mg $cm^{-2}$, and the gauze weighs 160 mg) leading to faster kinetics for the oxygen reduction reaction. Overall the performance is superior to that in the case of solid graphite backing only.

The *in situ* a.c. impedance characteristic (Cole–Cole plot) of the solid graphite-backing configuration is shown in Figure 7. It is characterized by a very large ohmic resistance and by a large kinetic semicircle indicating serious kinetic limitations. Using the new configuration (Figure 8), the kinetic resistance was decreased by a factor of 500. Notice also that in Figure 8 the ohmic resistance decreased by a factor of 2500. It is therefore legitimate to attribute the disintegration problem to deterioration of the electronic contact between the MEA and the backing during operation.

From Figure 9 it is evident that better kinetics are obtained using platinum gauze than using a metal backing of lesser activity for oxygen reduction, for example molybdenum. The ohmic resistance with molybdenum, however, is the same as with platinum.

### 3.5. *Energy consumption*

Figure 5b (Part I of this series [M.I. Ahmed et al., submitted]) showed the cell voltage required to sustain the operation at 0.2, 0.4, and 0.6 Å respectively, in the regeneration experiments. In all cases, the cell voltage increases with time, indicating an increase in cell resistance.

From measurements with a reference electrode during electrolysis at 0.2 Å, it appears that the anode voltage remained stable at 0.4–0.5 V vs $Hg/HgSO_4$, but the cathode voltage increases. This increase in the cathode voltage is attributed to flooding with water due to the liquid electrolyte permeation through the porous electrode, and metal deposition. The latter is not significant

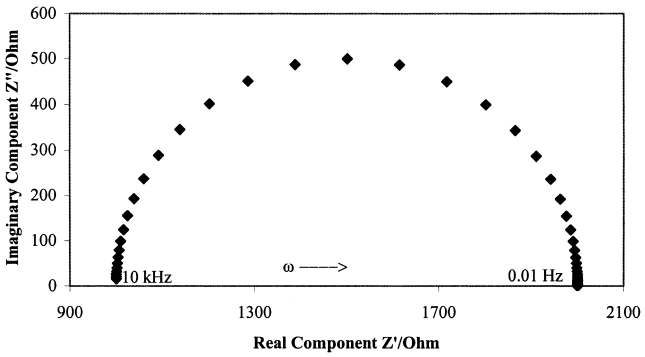


*Fig. 7.* A.c. impedance diagram (Cole–Cole plot) of the fuel cell cathode (old configuration) in contaminated chromic acid.

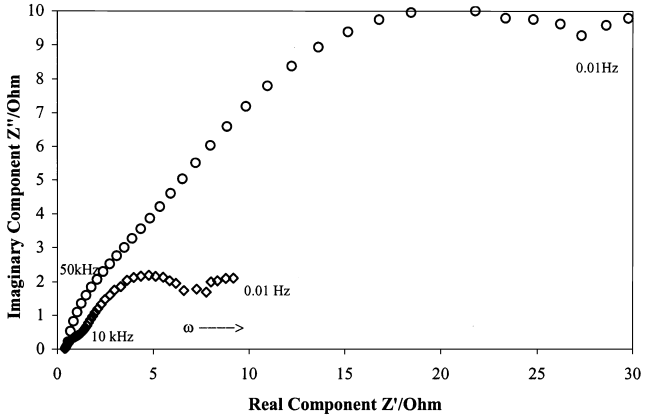


*Fig. 9.* A.c. impedance diagram (Cole–Cole plot) of the fuel cell cathode in contaminated chromic acid, using either molybdenum or platinum gauze as backing. (◇) Pt, (○) Mo.

in the case of low current densities but it appears to make a major contribution in the 0.4 and 0.6 Å current. The reason is that higher current densities as well as higher initial concentrations result in a higher fraction of the cathode reaction being associated with metal deposition.

After the modification of the backing configuration (Section 4 above), the cathode performance was much more stable and cell voltages of up to 3, 5, and 7 V, were obtained in a run of 5 days each for 0.2, 0.4, and 0.6 Å, respectively (Figure 5b in Part I of this series [M.I. Ahmed et al., submitted]). However reasonable these voltages might seem, they are two to three times higher than expected from thermodynamics, so further improvements could still be made.

## 4. Conclusions

It was found that the removal rate of contaminant metals is dependent on the strength of the electric field across the membrane, i.e., on the total cell current. At low total current, contaminant metals are not deposited at the cathode, but at higher total current, deposition of metals occurs. Though this may increase the removal rate, it is at the expense of a rising cell voltage.

Metal deposition within the porous electrode gives rise to kinetic limitations as well as increasing ohmic resistance, leading to higher energy requirements. In an improved design, therefore, metal deposition within the separation cell must be avoided, for example by a circulating catholyte design.

With a fully catalyzed cathode, an energy gain of at least 1.0 V, operating at 0.2 Å, is possible. However, even though they might reduce the removal efficiency, using poorly catalyzed electrodes may reduce the cost of the process compared to uncatalyzed electrodes.

## Acknowledgements

The authors would like to thank the EPA (project no. R 82-7125-01-0) and Dr S. Balakrishnan, Project Officer for their support in this study.

## References

1. E.A. Ticianelli, *J. Electroanal. Chem.* **387** (1995) 1.
2. K. Scott, W.M. Taama, S. Kramer, P. Argyropoulos and K. Sundmacher, *Electrochem. Acta* **45** (1999) 945.
3. T.E. Springer, M.S. Wilson and S. Gottesfeld, *J. Electrochem. Soc.* **140** (1993) 3513.
4. M. Giureanu and H. Wang, *J. Electrochem. Soc.* **146** (1999) 4031.
5. E. Avci, *Sep. Sci. Technol.* **24** (1989) 317.
6. P.N. Ross, Characterization of alloy electrocatalysts for direct oxidation of methanol. In 'Direct Methanol–Air Fuel Cells', ECS PV-92-14, A.R. Landgrebe, R.K. Sen and D.J. Wheeler (eds), 1992, pp. 51–69.
7. H.R. Kunz, The state-of-the-art hydrogen air phosphoric acid electrolyte fuel cells. In 'Electrode Materials and Process for Energy Conversion and Storage', ECS PV-77-6, J.D.E. McIntyre, S. Srinivasan and F.G. Will (eds), 1977, pp. 607–620.
8. P. Stonehart, *J. App. Electrochem.* **22** (1992) 995.
9. K. Kinoshita, Effect of sintering on porous fuel cell electrodes. In 'Direct Methanol–Air Fuel Cells', ECS PV-92-14, A.R. Landgrebe, R.K. Sen and D.J. Wheeler (eds), 1992, pp. 644–655.
10. S. Mukerjee and S. Srinivasan, *J. Electroan. Chem.* **357** (1993) 201.
11. T. Toda, H. Igaashi, H. Uchida and M. Watanabe, *J. Electrochem. Soc.* **146** (1999) 3750.
12. J.R. Chang, J.F. Lee, S.D. Lin and A.S. Lin, *J. Phys. Chem.* **99** (1995) 14798.